JCTC Journal of Chemical Theory and Computation

Article

pubs.acs.org/JCTC

State-Specific Embedding Potentials for Excitation-Energy Calculations

Csaba Daday,[†] Carolin König,[‡] Omar Valsson,[†] Johannes Neugebauer,*[,‡] and Claudia Filippi*[,†]

[†]MESA+ Institute for Nanotechnology, University of Twente, P.O. Box 217, 7500 AE Enschede, The Netherlands

[‡]Theoretische Organische Chemie, Organisch-Chemisches Institut, Westfälische Wilhelms-Universität Münster, Corrensstr. 40, 48149 Münster, Germany

Supporting Information

ABSTRACT: Embedding potentials are frequently used to describe the effect of an environment on the electronic structure of molecules in larger systems, including their excited states. If such excitations are accompanied by significant rearrangements in the electron density of the embedded molecule, large differential polarization effects may take place, which in turn can require state-specific embedding potentials for an accurate theoretical description. We outline here how to extend wave function in density functional theory (WF/DFT) methods to compute the excitation energies of a molecule in a responsive environment through the use of state-specific density-based embedding potentials constructed within a modified subsystem DFT approach. We evaluate the general expression of the ground- and excited-state energy difference of the total system both with the use of state-independent and state-dependent embedding potentials and propose some practical recipes to construct the approximate excited-state DFT density of the active part used to polarize the environment. We illustrate these concepts with the state-independent and state-dependent WF/DFT computation of the excitation energies of *p*-nitroaniline, acrolein, methylenecyclopropene, and *p*-nitrophenolate in various solvents.

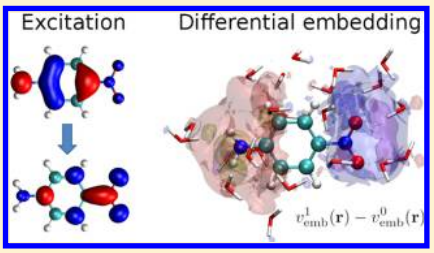

1. INTRODUCTION

A well-known strategy for electronic structure calculations on complex systems is to partition the system into an active region (system 1) and an environment (system 2) and then to employ a hybrid energy expression. In so-called additive hybrid schemes, the energy expression is written as

$$E^{\mathrm{hybrid}}_{(1+2)} = E^{M_A}_1 + E^{M_B}_2 + E^{M_C}_{(1\leftrightarrow 2)} \quad (1)$$

where $M_{A/B/C}$ denote the different theoretical methods used to calculate the energies of systems 1 and 2 and the interaction energy $E_{(1\leftrightarrow 2)}$. Often, methods M_B and M_C are identical. Several combinations of different methods are possible,[1−5] with the class of mixed quantum mechanics in molecular mechanics (QM/MM) methods being probably the most prominent ones.[1] In these methods, a polarization of system 1 due to the environment is achieved by including an embedding potential, in the simplest case just due to a set of point charges. If also the polarization of the environment by the active system shall be described, it is necessary to employ polarizable force fields.

Extensions for electronic excitations are also known in combination with the two standard ways of calculating excitation energies in electronic-structure theory,[6,7] namely, directly through a linear-response approach (i.e., as poles of the dynamic polarizability of the system) or as the difference between energies of two distinct electronic states of the combined system (1 + 2). Since the electron density of system 1 changes upon excitation, the mutual polarization between systems 1 and 2 will be different in the two electronic states. The resulting effect on excitation energies is known as the differential polarization. In response-based QM/MM methods, these effects can be described by including the response of the environment, for instance via induced dipole moments,[8−10] while, in energy-difference-based QM/MM methods, they can be easily obtained if polarizable MM models for the environment are employed: The polarization of the environment depends on the charge distribution of the embedded system, and changes in the charge distribution immediately lead to a change in the polarization. It should be emphasized that, in both theoretical frameworks, we aim at describing the combined or supersystem (1 + 2), so we want to describe either the response of the entire supersystem or a particular excited state of the supersystem in addition to its ground state.

Subsystem density-functional theory (DFT),[11,12] though in principle an alternative formulation of DFT, can be regarded as a hybrid method of Kohn−Sham (KS) DFT for systems 1 and 2 in which the interaction energy is calculated on the basis of orbital-free (OF) DFT.[13] By minimizing the total energy expression with respect to the density of system 1 (ρ_1) given a fixed density of the environment (ρ_2), one derives a set of Kohn−Sham-like equations for the optimal ρ_1, in which an effective embedding potential arises due to the presence of ρ_2.[14] Since the same can also be done for system 2, a scheme is derived in which systems 1 and 2 are iteratively polarized with respect to each other, until self-consistency.[15] In this way, subsystem DFT can be regarded as a fully self-consistent

Received: February 1, 2013
Published: March 27, 2013

   dx.doi.org/10.1021/ct400086a | J. Chem. Theory Comput. 2013, 9, 2355−2367

alternative to KS-DFT.[5,16] As far as excited-state calculations are concerned, the environmental response can be included in the corresponding response-based subsystem time-dependent density functional theory (TDDFT).[17−19]

Following the pioneering work by the Carter group,[20,21] several authors have dealt with the question of how to derive and numerically develop, in a similar spirit, wave function/density functional theory (WF/DFT) hybrid methods.[7,22−28] In these methods, density-based embedding potentials are used to include polarization effects[29] caused by the environment, while accurate correlated wave function methods can be employed for the active system. Both state-dependent[30−34] and response-based methods[35] have been suggested, which are in principle capable of capturing differential polarization. Although this issue has received significant attention in recent years, to the best of our knowledge, no numerical applications have been presented yet containing these contributions.

Here, we investigate possible routes for extending hybrid WF/DFT approaches for the calculation of excited states. We do not consider response-based approaches but concentrate on state-dependent methods. We will analyze different types of approximations that can or have to be made to make WF/DFT methods applicable in practice. We will compare the use of effective "embedding operators" in the calculation of the energy of system 1 with the explicit evaluation of the entire energy-difference expression. These approaches will be analyzed for state-independent (no differential polarization) and state-specific (differential polarization included) embedding potentials.

We will start with a presentation of the theory in section 2, followed by details of the implementation and computations in section 3. Results for a number of test cases are given in section 4 before we summarize our conclusions in section 5.

2. THEORY

2.1. DFT/DFT and WF/DFT Embedding Methods. We start by writing the subsystem DFT energy of a supersystem composed of two subsystems (1 and 2) as a DFT/DFT hybrid energy expression:

$$E_{(1+2)}^{\mathrm{DFT/DFT}} = E_1^{\mathrm{KS}}[\rho_1] + E_2^{\mathrm{KS}}[\rho_2] + E_{(1\leftrightarrow 2)}^{\mathrm{OFDFT}}[\rho_1, \rho_2] \tag{2}$$

The KS-DFT energies of systems 1 and 2 in this expression are

$$E_I^{\mathrm{KS}}[\rho_I] = T_s[\{\phi_{i_I}\}] + J[\rho_I] + V_{\mathrm{nuc},I}[\rho_I] + E_{\mathrm{xc}}[\rho_I] \tag{3}$$

where I denotes system 1 or 2, J is the Coulomb energy of a given electron density distribution, E_{xc} is the exchange−correlation energy, $V_{\mathrm{nuc},I}[\rho_I]$ is the interaction of the electron density of system I with the nuclei in the same system, and $T_s[\{\phi_{i_I}\}]$ is the kinetic energy as defined in the Kohn−Sham formalism, calculated from the Kohn−Sham-like orbitals, $\{\phi_{i_I}\}$. The interaction energy is then

$$E_{(1\leftrightarrow 2)}^{\mathrm{OFDFT}}[\rho_1, \rho_2] = V_{\mathrm{nuc},1}[\rho_2] + V_{\mathrm{nuc},2}[\rho_1] + J[\rho_1, \rho_2] + E_{\mathrm{xc}}^{\mathrm{nadd}}[\rho_1, \rho_2] + T_s^{\mathrm{nadd}}[\rho_1, \rho_2] \tag{4}$$

where $V_{\mathrm{nuc},I}[\rho_K]$ is the Coulomb attraction between the nuclei of system I and the electron density of system K, $J[\rho_1,\rho_2]$ is the Coulomb repulsion between the electron densities of the two systems,

$$J[\rho_1, \rho_2] = \int\int \frac{\rho_1(\mathbf{r}_1)\,\rho_2(\mathbf{r}_2)}{|\mathbf{r}_1 - \mathbf{r}_2|}\,\mathrm{d}\mathbf{r}_1\,\mathrm{d}\mathbf{r}_2 \tag{5}$$

and the nonadditive density functionals $F^{\mathrm{nadd}} = \{E_{\mathrm{xc}}^{\mathrm{nadd}}, T_s^{\mathrm{nadd}}\}$ are defined as

$$F^{\mathrm{nadd}}[\rho_1, \rho_2] = F[\rho_1 + \rho_2] - F[\rho_1] - F[\rho_2] \tag{6}$$

By minimizing eq 2 with respect to the density ρ_1 (keeping ρ_2 fixed), one obtains a set of Kohn−Sham-like equations containing an effective embedding potential[14]

$$v_{\mathrm{emb},1}(\mathbf{r}) = v_{\mathrm{nuc},2}(\mathbf{r}) + \int \frac{\rho_2(\mathbf{r}')}{|\mathbf{r} - \mathbf{r}'|}\,\mathrm{d}\mathbf{r}' + \frac{\delta E_{\mathrm{xc}}^{\mathrm{nadd}}[\rho_1, \rho_2]}{\delta \rho_1(\mathbf{r})} + \frac{\delta T_{\mathrm{xc}}^{\mathrm{nadd}}[\rho_1, \rho_2]}{\delta \rho_1(\mathbf{r})} \tag{7}$$

Here, $v_{\mathrm{nuc},2}$ is the Coulomb potential due to the nuclei of system 2. A similar embedding potential, $v_{\mathrm{emb},2}(\mathbf{r})$ (with indices 1 and 2 interchanged in $v_{\mathrm{emb},1}$) is obtained by minimizing the energy with respect to ρ_2. In practical applications, an iterative "freeze-and-thaw" scheme can be adopted in which systems 1 and 2 are mutually polarized until self-consistency.[15]

If the energy of system 1 shall be described in terms of a wave function method, we can, according to eq 1, employ the following WF/DFT energy expression

$$E_{(1+2)}^{\mathrm{WF/DFT}} = E_1^{\mathrm{WF}}[\Psi_1] + E_2^{\mathrm{KS}}[\rho_2] + E_{(1\leftrightarrow 2)}^{\mathrm{OFDFT}}[\rho_1, \rho_2] \tag{8}$$

with

$$E_1^{\mathrm{WF}}[\Psi_1] = \langle \Psi_1 | \{ \sum_i [-\frac{1}{2}\nabla_i^2 + v_{\mathrm{nuc},1}(\mathbf{r}_i)] + \sum_{i<j} \frac{1}{r_{ij}} \} | \Psi_1 \rangle \tag{9}$$

where the sum is over the electrons of system 1. In the WF/DFT context, the wave function Ψ_1 is obtained under the influence of the embedding potential $v_{\mathrm{emb},1}(\mathbf{r})$, i.e., with a modified one-electron operator[36]

$$\{ \sum_i [-\frac{1}{2}\nabla_i^2 + v_{\mathrm{nuc},1}(\mathbf{r}_i) + v_{\mathrm{emb},1}(\mathbf{r}_i)] + \sum_{i<j} \frac{1}{r_{ij}} \} \Psi_1 = \tilde{E}_1^{\mathrm{WF}} \Psi_1 \tag{10}$$

A similar embedding potential ($v_{\mathrm{emb},2}$) has to be included in the determination of ρ_2 within the KS-like equations for system 2. This potential depends on the density of system 1, so an iterative polarization of the active part and environment needs to be carried out, similar to the freeze-and-thaw scheme in the DFT/DFT context. Since this is usually very time-consuming and technically difficult with highly correlated WF methods, one can resort to approximate schemes in which the freeze-and-thaw cycles are carried out in a DFT/DFT embedding framework, and the resulting embedding potential is taken as an approximation for the fully self-consistent WF/DFT embedding potential.[37] As an alternative, Carter and co-workers have employed an environmental density ρ_2 which was calculated from a DFT-based density of the total system, from which the density of (isolated) system 1 was subtracted.[23]

2.2. Excitation Energies in WF/DFT. As mentioned before, we will only consider state-dependent electronic-structure methods here and thus not discuss response-based treatments. Excitation energies ΔE are therefore calculated explicitly as energy differences between excited and ground

electronic states. In the framework of WF/DFT embedding, this means

$$\Delta E = E^{\mathrm{WF/DFT}}_{(1+2)\mathrm{e}} - E^{\mathrm{WF/DFT}}_{(1+2)\mathrm{g}} \tag{11}$$

where the subscripts e and g refer to the excited and the ground state, respectively. The main question in this work is how to approximate the calculation of this energy difference and how different approximations affect the resulting excitation energies.

It has also been argued[7,32,35] and is physically reasonable that state-specific embedding potentials are needed for a consistent theoretical description of excitation energies in WF/DFT, which include differential polarization effects. In particular, Khait and Hoffmann pointed out that WF/DFT embedding is formally correct not only for ground but also for excited states.[32] They make use of the observation by Perdew and Levy in the context of pure DFT[38] that every extremum of the energy functional corresponds to a stationary-state density. Since, however, not every stationary-state density is also an extremum of the energy functional, the formal correctness only holds for a subset of excited states. In spite of this difficulty, we are going to investigate how a practical scheme for state-specific embedding potentials in WF/DFT calculations can be implemented, and whether the increased effort is justified by the results.

We will first neglect differential polarization effects. If the excitation is entirely localized within the embedded system (system 1), it is often a good approximation to assume that system 2 does not respond to the excitation of system 1 so that the density ρ_2 is the same in both calculations. The embedding potentials for ground- and excited-state calculations derived from ρ_2 will also be very similar since the (often dominant) electrostatic contribution is unchanged. However, they will not be precisely the same since the nonadditive parts of the orbital-free embedding potential depend also on ρ_1, which is different for the two states. In addition, one can further approximate the DFT-based embedding potential by calculating it from a fixed guess for the density of the active system,[39] a strategy that has been used in the context of WF/DFT embedding before.[37] This has the advantage that the embedding potential can be generated on a grid, and then be reused in both the ground- and excited-state calculations.

Writing the energy difference explicitly with the assumption of no differential polarization (ρ_2 unchanged), we obtain

$$\begin{aligned}\Delta E^{\text{no-dpol}} &= (E_1^{\mathrm{WF}}[\Psi_1^{\mathrm{e}}] + E_2^{\mathrm{KS}}[\rho_2] + E^{\mathrm{OFDFT}}_{(1\leftrightarrow 2)}[\rho_1^{\mathrm{e}}, \rho_2]) \\ &\quad - (E_1^{\mathrm{WF}}[\Psi_1^{\mathrm{g}}] + E_2^{\mathrm{KS}}[\rho_2] + E^{\mathrm{OFDFT}}_{(1\leftrightarrow 2)}[\rho_1^{\mathrm{g}}, \rho_2]) \\ &= E_1^{\mathrm{WF}}[\Psi_1^{\mathrm{e}}] + E^{\mathrm{OFDFT}}_{(1\leftrightarrow 2)}[\rho_1^{\mathrm{e}}, \rho_2] \\ &\quad - E_1^{\mathrm{WF}}[\Psi_1^{\mathrm{g}}] - E^{\mathrm{OFDFT}}_{(1\leftrightarrow 2)}[\rho_1^{\mathrm{g}}, \rho_2]\end{aligned} \tag{12}$$

where we denote the ground- and excited-state wave functions with Ψ_1^{g} and Ψ_1^{e}, and the corresponding densities with ρ_1^{g} and ρ_1^{e}. Note that, in addition to $E_2^{\mathrm{KS}}[\rho_2]$, the term $V_{\mathrm{nuc},1}[\rho_2]$ contained in $E^{\mathrm{OFDFT}}_{(1\leftrightarrow 2)}$ will also cancel out in the above expression.

If we considered only electrostatic interaction terms, i.e. neglected all differential nonadditive terms, then the excitation energy would be

$$\begin{aligned}\Delta E^{\mathrm{elstat}} &= (E_1^{\mathrm{WF}}[\Psi_1^{\mathrm{e}}] - E_1^{\mathrm{WF}}[\Psi_1^{\mathrm{g}}]) + V_{\mathrm{nuc},2}[\rho_1^{\mathrm{e}}] - V_{\mathrm{nuc},2}[\rho_1^{\mathrm{g}}] \\ &\quad + J[\rho_1^{\mathrm{e}}, \rho_2] - J[\rho_1^{\mathrm{g}}, \rho_2] \\ &= (E_1^{\mathrm{WF}}[\Psi_1^{\mathrm{e}}] - E_1^{\mathrm{WF}}[\Psi_1^{\mathrm{g}}]) + \langle\Psi_1^{\mathrm{e}}|\sum_i v^{\mathrm{elstat}}_{\mathrm{emb},1}(\mathbf{r}_i)|\Psi_1^{\mathrm{e}}\rangle \\ &\quad - \langle\Psi_1^{\mathrm{g}}|\sum_i v^{\mathrm{elstat}}_{\mathrm{emb},1}(\mathbf{r}_i)|\Psi_1^{\mathrm{g}}\rangle\end{aligned} \tag{13}$$

where we introduced the electrostatic component of the embedding potential

$$v^{\mathrm{elstat}}_{\mathrm{emb},1}(\mathbf{r}) = v_{\mathrm{nuc},2}(\mathbf{r}) + \int \frac{\rho_2(\mathbf{r}')}{|\mathbf{r} - \mathbf{r}'|}\,\mathrm{d}\mathbf{r}' \tag{14}$$

Evaluating excitation energies according to eq 13 would be particularly simple since it corresponds to computing the differences of the modified energies $\tilde{E}_1^{\mathrm{WF}}$ from eq 10 (only considering the electrostatic contribution in the embedding potential).

It is thus appealing to compute approximate excitation energies from WF/DFT as a simple difference in the ground- and excited-state eigenvalues of a modified Hamiltonian including the (ground-state-like) embedding potential as in eq 10, now containing all contributions

$$\begin{aligned}\Delta E^{(A)}_{\mathrm{approx}} &= E_1^{\mathrm{WF}}[\Psi_1^{\mathrm{e}}] + \langle\Psi_1^{\mathrm{e}}|\sum_i v_{\mathrm{emb},1}(\mathbf{r}_i)|\Psi_1^{\mathrm{e}}\rangle \\ &\quad - E_1^{\mathrm{WF}}[\Psi_1^{\mathrm{g}}] - \langle\Psi_1^{\mathrm{g}}|\sum_i v_{\mathrm{emb},1}(\mathbf{r}_i)|\Psi_1^{\mathrm{g}}\rangle \\ &= E_1^{\mathrm{WF}}[\Psi_1^{\mathrm{e}}] - E_1^{\mathrm{WF}}[\Psi_1^{\mathrm{g}}] + V_{\mathrm{nuc},2}[\rho_1^{\mathrm{e}}] - V_{\mathrm{nuc},2}[\rho_1^{\mathrm{g}}] \\ &\quad + J[\rho_1^{\mathrm{e}}, \rho_2] - J[\rho_1^{\mathrm{g}}, \rho_2] \\ &\quad + \int v_{\mathrm{xc}}^{\mathrm{nadd}}[\rho_1^{\mathrm{g}}, \rho_2](\mathbf{r})[\rho_1^{\mathrm{e}}(\mathbf{r}) - \rho_1^{\mathrm{g}}(\mathbf{r})]\,\mathrm{d}\mathbf{r} \\ &\quad + \int v_t^{\mathrm{nadd}}[\rho_1^{\mathrm{g}}, \rho_2](\mathbf{r})[\rho_1^{\mathrm{e}}(\mathbf{r}) - \rho_1^{\mathrm{g}}(\mathbf{r})]\,\mathrm{d}\mathbf{r}\end{aligned} \tag{15}$$

where we denote the ground- and excited-state wave functions in the potential $v_{\mathrm{emb},1}$ [eq 10] with Ψ_1^{g} and Ψ_1^{e}, and the corresponding densities with ρ_1^{g} and ρ_1^{e}. The potentials $v_{\mathrm{xc}}^{\mathrm{nadd}}$ and v_t^{nadd} are the functional derivatives of the corresponding energy functionals as appearing in eq 7. The use of a ground-state-like embedding potential in the ground- and excited-state WF calculations will be denoted as route (A) in the following. It is equivalent to the "first-order corrected" approach employed by Carter and co-workers in ref 34, while they used the approximation

$$\Delta E^{\text{no-dpol}} \approx E_1^{\mathrm{WF}}[\Psi_1^{\mathrm{e}}] - E_1^{\mathrm{WF}}[\Psi_1^{\mathrm{g}}] \tag{16}$$

in their earlier work.[30,31,33] This older approximation does however not contain the change in the electrostatic interaction contributions between the subsystems, which has been shown to substantially affect the excitation energies of Mg_nO_n clusters.[34]

2.3. State-Specific vs State-Independent Embedding.

A second route in our current work—denoted with (B)—is to allow system 2 to respond to the excitation of 1, and in turn to include "back" polarization effects on system 1. This is equivalent to saying that the energy difference contains differential polarization effects, which requires state-specific embedding potentials.

We rewrite the general expression of the energy of the total system in an excited state localized on system 1 as

$$E^{\mathrm{WF/DFT}}_{(1+2)\mathrm{e}} = E^{\mathrm{WF}}_1[\tilde{\Psi}^{\mathrm{e}}_1] + E^{\mathrm{KS}}_2[\tilde{\rho}_2] + E^{\mathrm{OFDFT}}_{(1\leftrightarrow 2)}[\tilde{\rho}^{\mathrm{e}}_1, \tilde{\rho}_2] \quad (17)$$

where $\tilde{\Psi}^{\mathrm{e}}_1$ denotes the excited-state wave function computed in an embedding potential which accounts for differential polarization. In principle, all energy expressions for ground and excited states have to be evaluated with self-consistently optimized subsystem densities/wave functions[32] so that also the energy of system 2 and the interaction energy in the above expression differ from the ones in the ground-state case, eq 8. We denote these general, self-consistent quantities entering in eq 17 with a tilde and discuss below some specific, practical choices for their computation.

The general excitation energy is given by the difference between this WF/DFT excited-state energy and the ground-state one of eq 8:

$$\begin{aligned}\Delta E &= E^{\mathrm{WF/DFT}}_{(1+2)\mathrm{e}} - E^{\mathrm{WF/DFT}}_{(1+2)\mathrm{g}} \\ &= E^{\mathrm{WF}}_1[\tilde{\Psi}^{\mathrm{e}}_1] - E^{\mathrm{WF}}_1[\Psi^{\mathrm{g}}_1] + E^{\mathrm{KS}}_2[\tilde{\rho}_2] - E^{\mathrm{KS}}_2[\rho_2] \\ &\quad + E^{\mathrm{OFDFT}}_{(1\leftrightarrow 2)}[\tilde{\rho}^{\mathrm{e}}_1, \tilde{\rho}_2] - E^{\mathrm{OFDFT}}_{(1\leftrightarrow 2)}[\rho^{\mathrm{g}}_1, \rho_2] \\ &= E^{\mathrm{WF}}_1[\tilde{\Psi}^{\mathrm{e}}_1] - E^{\mathrm{WF}}_1[\Psi^{\mathrm{g}}_1] + E^{\mathrm{KS}}_2[\tilde{\rho}_2] - E^{\mathrm{KS}}_2[\rho_2] \\ &\quad + V_{\mathrm{nuc},1}[\tilde{\rho}_2] - V_{\mathrm{nuc},1}[\rho_2] + V_{\mathrm{nuc},2}[\tilde{\rho}^{\mathrm{e}}_1] - V_{\mathrm{nuc},2}[\rho^{\mathrm{g}}_1] \\ &\quad + J[\tilde{\rho}^{\mathrm{e}}_1, \tilde{\rho}_2] - J[\rho^{\mathrm{g}}_1, \rho_2] + E^{\mathrm{nadd}}_{\mathrm{xc}}[\tilde{\rho}^{\mathrm{e}}_1, \tilde{\rho}_2] \\ &\quad - E^{\mathrm{nadd}}_{\mathrm{xc}}[\rho^{\mathrm{g}}_1, \rho_2] + T^{\mathrm{nadd}}_s[\tilde{\rho}^{\mathrm{e}}_1, \tilde{\rho}_2] - T^{\mathrm{nadd}}_s[\rho^{\mathrm{g}}_1, \rho_2]\end{aligned} \quad (18)$$

where, for clarity, we denote the ground-state solutions for system 1 in eq 8 as Ψ^{g}_1 and ρ^{g}_1.

For both cases (A) and (B), the practical implementation of the ground-state energy calculations is the same: Following for instance ref 37, we do not employ the WF density of system 1 but perform an iterative "freeze-and-thaw" scheme within subsystem DFT, in which systems 1 and 2 are mutually polarized in the ground state until self-consistency. We then construct an embedding potential $v_{\mathrm{emb},1}(\mathbf{r})$ based on the final ground-state DFT densities of systems 1 and 2 to obtain the embedded ground-state wave function Ψ^{g}_1 of system 1.

For the excited-state calculation in case (A), the ground-state-like embedding potential $v_{\mathrm{emb},1}(\mathbf{r})$ is also used to calculate an excited-state wave function, $\tilde{\Psi}^{\mathrm{e}}_1 = \Psi^{\mathrm{e}}_1$, and the corresponding density $\tilde{\rho}^{\mathrm{e}}_1 = \rho^{\mathrm{e}}_1$. The density of system 2 remains unchanged so that $\tilde{\rho}_2 = \rho_2$. The excitation energy in case (A) can be calculated as

$$\begin{aligned}\Delta E^{(\mathrm{A})} &= E^{\mathrm{WF}}_1[\Psi^{\mathrm{e}}_1] - E^{\mathrm{WF}}_1[\Psi^{\mathrm{g}}_1] + V_{\mathrm{nuc},2}[\rho^{\mathrm{e}}_1] - V_{\mathrm{nuc},2}[\rho^{\mathrm{g}}_1] \\ &\quad + J[\rho^{\mathrm{e}}_1, \rho_2] - J[\rho^{\mathrm{g}}_1, \rho_2] + E^{\mathrm{nadd}}_{\mathrm{xc}}[\rho^{\mathrm{e}}_1, \rho_2] \\ &\quad - E^{\mathrm{nadd}}_{\mathrm{xc}}[\rho^{\mathrm{g}}_1, \rho_2] + T^{\mathrm{nadd}}_s[\rho^{\mathrm{e}}_1, \rho_2] - T^{\mathrm{nadd}}_s[\rho^{\mathrm{g}}_1, \rho_2]\end{aligned} \quad (19)$$

where the $E^{\mathrm{KS}}_2[\rho_2]$ and $V_{\mathrm{nuc},1}[\rho_2]$ terms cancel in the difference of the interaction energies. If we compare $\Delta E^{(\mathrm{A})}$ with the approximate expression (eq 15), we observe that the electrostatic interaction terms, which often dominate environment effects on excitation energies, are treated exactly in $\Delta E^{(\mathrm{A})}_{\mathrm{approx}}$ (for the given densities), and that the approximation in eq 15 amounts to neglecting the following correction term:

$$\begin{aligned}\delta E^{(\mathrm{A})}_{\mathrm{nadd}} &= \Delta E^{(\mathrm{A})} - \Delta E^{(\mathrm{A})}_{\mathrm{approx}} \\ &= E^{\mathrm{nadd}}_{\mathrm{xc}}[\rho^{\mathrm{e}}_1, \rho_2] - E^{\mathrm{nadd}}_{\mathrm{xc}}[\rho^{\mathrm{g}}_1, \rho_2] + T^{\mathrm{nadd}}_s[\rho^{\mathrm{e}}_1, \rho_2] \\ &\quad - T^{\mathrm{nadd}}_s[\rho^{\mathrm{g}}_1, \rho_2] - \int \{v^{\mathrm{nadd}}_{\mathrm{xc}}[\rho^{\mathrm{g}}_1, \rho_2](\mathbf{r}) \\ &\quad + v^{\mathrm{nadd}}_t[\rho^{\mathrm{g}}_1, \rho_2](\mathbf{r})\}[\rho^{\mathrm{e}}_1(\mathbf{r}) - \rho^{\mathrm{g}}_1(\mathbf{r})]\, \mathrm{d}\mathbf{r}\end{aligned} \quad (20)$$

Although there is no rigorous justification for this approximation, we observe that (i) all ingredients here are "non-additive" terms, which go to zero for noninteracting systems and will be small for weakly interacting systems, (ii) we are taking differences between these terms evaluated with very similar (or even equal, for ρ_2) densities, and (iii) exchange–correlation and kinetic-energy contributions often cancel out to a certain degree. Therefore, this approximation can be expected to be rather good in practical applications.

For the excited-state calculation in case (B), where the WF/DFT hybrid scheme is improved by considering differential polarization effects, we construct a new embedding potential $v^{\mathrm{pol}}_{\mathrm{emb},2}(\mathbf{r})$ based on an approximate excited-state density of system 1. With this potential, we calculate a ground-state density $\tilde{\rho}_2 = \rho^{\mathrm{pol}}_2(\mathbf{r})$ that is polarized with respect to the excited-state density of system 1. Then, we use $\rho^{\mathrm{pol}}_2(\mathbf{r})$ to construct an excited-state-like embedding potential $v^{\mathrm{pol,e}}_{\mathrm{emb},1}(\mathbf{r})$, and then iterate until self-consistency. The final $v^{\mathrm{pol,e}}_{\mathrm{emb},1}(\mathbf{r})$ is employed to calculate an excited-state wave function, $\tilde{\Psi}^{\mathrm{e}}_1 = \Psi^{\mathrm{pol,e}}_1$, and corresponding density $\tilde{\rho}^{\mathrm{e}}_1 = \rho^{\mathrm{pol,e}}_1(\mathbf{r})$. The full excitation-energy expression is

$$\begin{aligned}\Delta E^{(\mathrm{B})} &= E^{\mathrm{WF}}_1[\Psi^{\mathrm{pol,e}}_1] - E^{\mathrm{WF}}_1[\Psi^{\mathrm{g}}_1] + E^{\mathrm{KS}}_2[\rho^{\mathrm{pol}}_2] - E^{\mathrm{KS}}_2[\rho_2] \\ &\quad + V_{\mathrm{nuc},1}[\rho^{\mathrm{pol}}_2] - V_{\mathrm{nuc},1}[\rho_2] + V_{\mathrm{nuc},2}[\rho^{\mathrm{pol,e}}_1] - V_{\mathrm{nuc},2}[\rho^{\mathrm{g}}_1] \\ &\quad + J[\rho^{\mathrm{pol,e}}_1, \rho^{\mathrm{pol}}_2] - J[\rho^{\mathrm{g}}_1, \rho_2] + E^{\mathrm{nadd}}_{\mathrm{xc}}[\rho^{\mathrm{pol,e}}_1, \rho^{\mathrm{pol}}_2] \\ &\quad - E^{\mathrm{nadd}}_{\mathrm{xc}}[\rho^{\mathrm{g}}_1, \rho_2] + T^{\mathrm{nadd}}_s[\rho^{\mathrm{pol,e}}_1, \rho^{\mathrm{pol}}_2] - T^{\mathrm{nadd}}_s[\rho^{\mathrm{g}}_1, \rho_2]\end{aligned} \quad (21)$$

where the situation changes with respect to case (A) as the energy contributions for system 2 do not cancel anymore.

In analogy to case (A), the approximate form of the excitation energy where the system-interaction is accounted for via expectation values of embedding potentials is given by

$$\begin{aligned}\Delta E^{(\mathrm{B})}_{\mathrm{approx}} &= E^{\mathrm{WF}}_1[\Psi^{\mathrm{pol,e}}_1] + \langle \Psi^{\mathrm{pol,e}}_1 | \sum_i v^{\mathrm{pol,e}}_{\mathrm{emb},1}(\mathbf{r}_i) | \Psi^{\mathrm{pol,e}}_1 \rangle \\ &\quad - E^{\mathrm{WF}}_1[\Psi^{\mathrm{g}}_1] - \langle \Psi^{\mathrm{g}}_1 | \sum_i v_{\mathrm{emb},1}(\mathbf{r}_i) | \Psi^{\mathrm{g}}_1 \rangle \\ &= E^{\mathrm{WF}}_1[\Psi^{\mathrm{pol,e}}_1] - E^{\mathrm{WF}}_1[\Psi^{\mathrm{g}}_1] + V_{\mathrm{nuc},2}[\rho^{\mathrm{pol,e}}_1] \\ &\quad - V_{\mathrm{nuc},2}[\rho^{\mathrm{g}}_1] + J[\rho^{\mathrm{pol,e}}_1, \rho^{\mathrm{pol}}_2] - J[\rho^{\mathrm{g}}_1, \rho_2] \\ &\quad + \int \{v^{\mathrm{nadd}}_{\mathrm{xc}}[\rho^{\mathrm{pol,e}}_1, \rho^{\mathrm{pol}}_2](\mathbf{r}) \\ &\quad + v^{\mathrm{nadd}}_t[\rho^{\mathrm{pol,e}}_1, \rho^{\mathrm{pol}}_2](\mathbf{r})\} \rho^{\mathrm{pol,e}}_1(\mathbf{r})\, \mathrm{d}\mathbf{r} \\ &\quad - \int \{v^{\mathrm{nadd}}_{\mathrm{xc}}[\rho^{\mathrm{g}}_1, \rho_2](\mathbf{r}) \\ &\quad + v^{\mathrm{nadd}}_t[\rho^{\mathrm{g}}_1, \rho_2](\mathbf{r})\} \rho^{\mathrm{g}}_1(\mathbf{r})\, \mathrm{d}\mathbf{r}\end{aligned} \quad (22)$$

Even if we assume that we can disregard all differential kinetic-energy and exchange–correlation terms appearing as corrections to $E^{\mathrm{WF}}_1[\Psi^{\mathrm{pol,e}}_1] - E^{\mathrm{WF}}_1[\Psi^{\mathrm{g}}_1]$, we still make the following approximation compared to the full excited-state expression [eq 21]:

$$E_2^{KS}[\rho_2^{pol}] - E_2^{KS}[\rho_2] + V_{nuc,1}[\rho_2^{pol}] - V_{nuc,1}[\rho_2] \approx 0 \quad (23)$$

which is, as far as the electrostatic terms are concerned, equivalent to the following approximation:

$$\int \{v_{Coul}[\rho_2 + \Delta\rho_2/2](\mathbf{r}) + v_{nuc,1}(\mathbf{r}) + v_{nuc,2}(\mathbf{r})\}\Delta\rho_2(\mathbf{r})\, d\mathbf{r} \approx 0 \quad (24)$$

where $\Delta\rho_2(\mathbf{r}) = \rho_2^{pol}(\mathbf{r}) - \rho_2(\mathbf{r})$. This may be a rather drastic approximation, leading to errors on the same order of magnitude as the environment-induced shift that shall be calculated.

Our analysis reveals however a simple, practical cure to account for differential polarization effects and to remain within an approximation of the style of eq 22. We stress that the use of such an expression is, from a pragmatic point of view, preferable over the computation of the true excitation energy [eq 21] since the one-electron integrals in the WF calculation can be used both in the variational optimization of the wave function and in the energy calculation. The use of eq 21 requires instead first to optimize the wave functions with the corresponding embedding potential and then to evaluate the energy expression without it. Fortunately, a simple solution is possible whose ingredients are to (i) calculate the change in the energy in system 2 explicitly and (ii) correct for the remaining Coulomb error, which leads to the simple correction

$$\delta E_{simple}^{(B)} = E_2^{KS}[\rho_2^{pol}] - E_2^{KS}[\rho_2] + \int v_{nuc,1}(\mathbf{r})\, \Delta\rho_2(\mathbf{r})\, d\mathbf{r} \quad (25)$$

An improved excitation energy with state-specific embedding potentials can then be obtained as

$$\begin{aligned}\Delta E_{simple}^{(B)} &= \Delta E_{approx}^{(B)} + \delta E_{simple}^{(B)} \\ &= E_1^{WF}[\Psi_1^{pol,e}] + \langle\Psi_1^{pol,e}| \sum_i v_{emb,1}^{pol,e}(\mathbf{r}_i)|\Psi_1^{pol,e}\rangle \\ &\quad - E_1^{WF}[\Psi_1^{g}] - \langle\Psi_1^{g}| \sum_i v_{emb,1}(\mathbf{r}_i)|\Psi_1^{g}\rangle \\ &\quad + E_2^{KS}[\rho_2^{pol}] - E_2^{KS}[\rho_2] \\ &\quad + \int v_{nuc,1}(\mathbf{r})\Delta\rho_2(\mathbf{r})\, d\mathbf{r}\end{aligned} \quad (26)$$

The remaining approximations are consistent with the ones made in eq 15 for a state-independent embedding potential, and to assess their impact, we can explicitly calculate the neglected terms

$$\begin{aligned}\delta E_{nadd}^{(B)} &= E_{xc}^{nadd}[\rho_1^{pol,e}, \rho_2^{pol}] - E_{xc}^{nadd}[\rho_1^{g}, \rho_2] + T_s^{nadd}[\rho_1^{pol,e}, \rho_2^{pol}] \\ &\quad - T_s^{nadd}[\rho_1^{g}, \rho_2] - \int \{v_{xc}^{nadd}[\rho_1^{pol,e}, \rho_2^{pol}](\mathbf{r}) \\ &\quad + v_t^{nadd}[\rho_1^{pol,e}, \rho_2^{pol}](\mathbf{r})\}\rho_1^{pol,e}(\mathbf{r})\, d\mathbf{r} \\ &\quad + \int \{v_{xc}^{nadd}[\rho_1^{g}, \rho_2](\mathbf{r}) + v_t^{nadd}[\rho_1^{g}, \rho_2](\mathbf{r})\}\rho_1^{g}(\mathbf{r})\, d\mathbf{r}\end{aligned} \quad (27)$$

As mentioned above, in both schemes (A) and (B), we will introduce an additional approximation in practice and resort to the use of subsystem DFT densities for systems 1 and 2 to compute the embedding potentials needed in the WF/DFT calculations. For the ground-state calculations in both schemes, we follow the practical route to self-consistently converge the ground-state subsystem DFT densities of both systems, which are then used to construct the embedding potential, $v_{emb,1}(r)$, for the ground-state WF calculation of system 1. Similarly, for the excited-state calculation of scheme (B), we construct the excited-state-like embedding potential, $v_{emb,1}^{pol,e}(\mathbf{r})$, from an approximate excited-state embedded DFT density of system 1 and the polarized ground-state DFT density of system 2, which are obtained self-consistently. In section 4.1, we discuss two simple possible choices for approximate embedded excited-state DFT densities.

3. COMPUTATIONAL DETAILS

To optimize the structures, we use either the Gaussian 09[40] or the Turbomole code, version 6.0.[41] We employ density functional theory (DFT) and the cc-pVDZ[42] basis set in combination with the B3LYP[43,44] functional for *p*-nitroaniline and the BLYP[45,46] functional for all other molecules.

All subsystem DFT calculations are performed using the ADF package.[47] We employ the M06-HF[48] exchange-correlation functional and the DZP[49] basis set. For the frozen-density embedding calculations, we use the PW91k kinetic-energy functional[50] to compute the nonadditive terms of the kinetic energy since this functional has been shown to give a good performance in frozen density embedding.[51] For the nonadditive exchange-correlation contribution, we employ the local density approximation (LDA)[52] since, in ADF, we cannot use the nonlocal M06-HF functional for this term as done in the intrasubsystem calculations. We have tested the use of PW91, instead of LDA, for all four molecules and found that the excitation energies within scheme (A) vary by less than 0.05 eV.

We perform the complete-active-space self-consistent field (CASSCF) and second-order perturbation theory (CASPT2) calculations using MOLCAS 7.4.[53] For the CASSCF/DFT and CASPT2/DFT embedding calculations, we use a modified version of the MOLCAS code where the embedding interface is adapted from the Molcas-Embed interface developed by Carter and co-workers.[23,54] We use state-averaged CASSCF wave functions with equal weights on the ground and the excited states of interest and report below the single-state CASPT2 excitation energies. In the CASPT2 calculations, we employ the default IPEA zero-order Hamiltonian[55] and introduce an additional constant imaginary shift[56] of 0.1 au. In the CASPT2 calculations, we freeze the lowest σ orbitals corresponding to the 1s atomic orbitals of the heavy atoms in the system. We use the Cholesky decomposition of the two-electron integrals[57] with the threshold of 10^{-4}. The default convergence criteria are used for all calculations.

In all CASSCF and CASPT2 calculations, the aug-cc-pVDZ[42,58] basis set is used for the solvated molecule, and in the supermolecular calculations, a 6-31G[59] basis set is employed for the solvent molecules. To test the basis-set convergence, we compute the CASPT2 excitation energies of the *p*-nitroaniline with state-independent embedding potentials (case A) with the aug-cc-pVTZ basis set[42,58] and find a decrease by at most 0.05 eV with respect to the use of the aug-cc-pVDZ.

In the QM/MM calculations, we use the TIP3P[60] values of $q_O = -0.834e$ and $q_H = 0.417e$ when treating the water molecules as nonpolarizable point charges.

4. RESULTS

To illustrate the performance of the WF/DFT embedding schemes discussed above, we consider the four molecules shown in Figure 1, that is, *p*-nitroaniline (PNA), *s*-cis-acrolein,

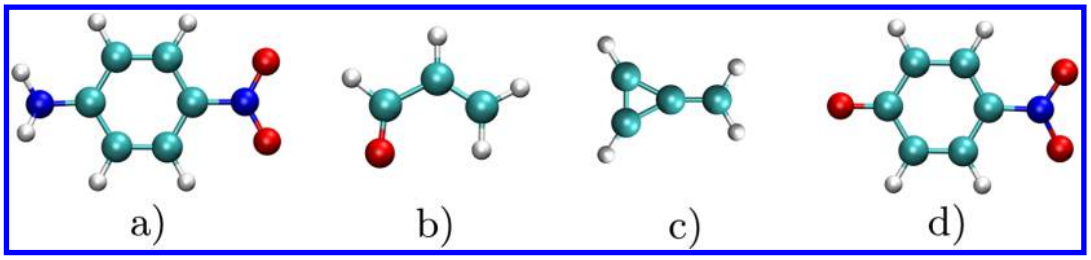

Figure 1. The solvated molecules considered in this work: (a) *p*-nitroaniline (PNA), (b) *s*-cis-acrolein, (c) methylenecyclopropene (MCP), and (d) *p*-nitrophenolate (PNP).

methylenecyclopropene (MCP), and the anionic *p*-nitrophenolate (PNP). For each molecule, we construct a model cluster consisting of the molecule solvated in a small number of waters as detailed in Table 1. For acrolein, we also consider as solvents methylamine (CH_3NH_2), carbon-tetrachloride (CCl_4), and cyclohexane (C_6H_{12}). The cluster models for acrolein in the four solvents are shown in Figure 2.

Table 1. Solute Molecules and Corresponding Solvents[a]

solute		solvent	CAS(n,m)	SA
PNA	22	H_2O	12,10	2
acrolein	19	H_2O	6,7	3
	10	CH_3NH_2	6,7	3
	6	CCl_4	6,7	3
	6	C_6H_{12}	6,7	3,5
MCP	17	H_2O	4,4	2
PNP	26	H_2O	12,10	2

[a]The number of solvent molecules included in the solute−solvent cluster model is indicated. We also list the dimension of the CAS expansion with the number n of electrons in m active orbitals, which we employ in the wave function calculations, and the number of states included in the state-averaged (SA) calculations.

The choice of these four molecules is motivated by different reasons. PNA represents a perfect test case for our study since its lowest singlet $\pi \rightarrow \pi^*$ excitation is characterized by strong intramolecular charge transfer and the response of the solvent environment is expected to be significant, leading to a shift of about 1 eV in the excitation energy in water solution with respect to the gas phase.[61,62] Acrolein is an interesting molecule since it has both conjugated double bonds and lone-pair electrons with the two lowest singlet excitations being of different character ($n \rightarrow \pi^*$ and $\pi \rightarrow \pi^*$). Furthermore, these two transitions respond in an opposite fashion to a polar solvent like water, with the corresponding excitation energies displaying a blue and a red shift, respectively, with respect to the gas phase.[63] The MCP molecule is also a potentially promising test case since its properties change rather dramatically upon photoexcitation. For instance, in the vertical $\pi \rightarrow \pi^*$ transition, the dipole moments of the ground and excited states have opposite signs and the solvatochromic shift in water is expected to be significant and on the order of 0.5 eV.[64] Finally, the anionic PNP has been recently studied with the aid of polarizable force fields, and it has been reported that the mutual polarization between PNP and the water solvent accounts for a large part (0.2−0.3 eV) of the shift in the excitation energy with respect to the gas phase.[9]

As the WF method, we employ the multireference perturbation theory approach (CASPT2) both to compute the excitation energies of the solvated molecule in an embedding potential as well as to perform the so-called supermolecular calculations, where the solvation shell is included in the active region and treated at the WF level. In the systems considered here, the excitations are predominantly localized on the solvated molecules and are therefore not characterized by charge transfer to the solvent. Consequently, also in the supermolecular calculations, the excitations can be described with the use of a CAS expansion constructed from a set of orbitals mainly localized on the molecule itself.

For all $\pi \rightarrow \pi^*$ excitations, we employ a minimal CAS expansion comprising all π electrons in the reference and a number of active orbitals equal to the number of heavy atoms as obtained by using one atomic orbital of p character per heavy atom. For acrolein, since we compute both the $n \rightarrow \pi^*$ and the $\pi \rightarrow \pi^*$ excitation energies, we use at least 3 states in the state-averaged (SA) calculations and extend the active space to include two lone-pair electrons on the oxygen as well as two additional n and π antibonding orbitals. For a given system, we employ the same active space and number of states in the state-averaged calculations both in the subsystem and in the supermolecular calculations as detailed in Table 1. For acrolein in cyclohexane, we employ 3 and 5 states in the supermolecular and embedding calculations, respectively, since the relevant states in the latter become the second and the fourth.

4.1. Excited-State DFT Density. The construction of the embedding potential in the WF/DFT calculations requires an approximation for the density of both the active system and the environment. In case (A), we use the same strategy as in ref 37; i.e., we utilize the densities obtained in a subsystem DFT treatment for the ground state of both systems. In case (B), we want to relax the environment within subsystem DFT in the presence of a solvated molecule in its excited state and must therefore construct an approximate DFT density of the excited state of the solute. Here, we test two simple procedures, which lead to two different approximate densities named here self-consistent post-Kohn−Sham (scp-KS) and fully relaxed (fr-KS) densities.

In both schemes for case (B), we assume that the excitation is of pure single-orbital transition nature. We therefore start from the ground-state Kohn−Sham orbitals and modify the occupation numbers by moving an electron from an occupied to a virtual orbital with a 0.5 fractional occupation of the up- and down-spin components in both orbitals. Here, we generally focus on the lowest singlet excitation where one electron is promoted from the HOMO to the LUMO orbital. The only exception is the $n \rightarrow \pi^*$ excitation in acrolein, which is a transition from the HOMO−1 to the LUMO orbital at the KS level. In the scp-KS scheme, the orbitals of the molecules are not further relaxed, so the excited-state density is simply constructed with fractionally occupied ground-state orbitals. In

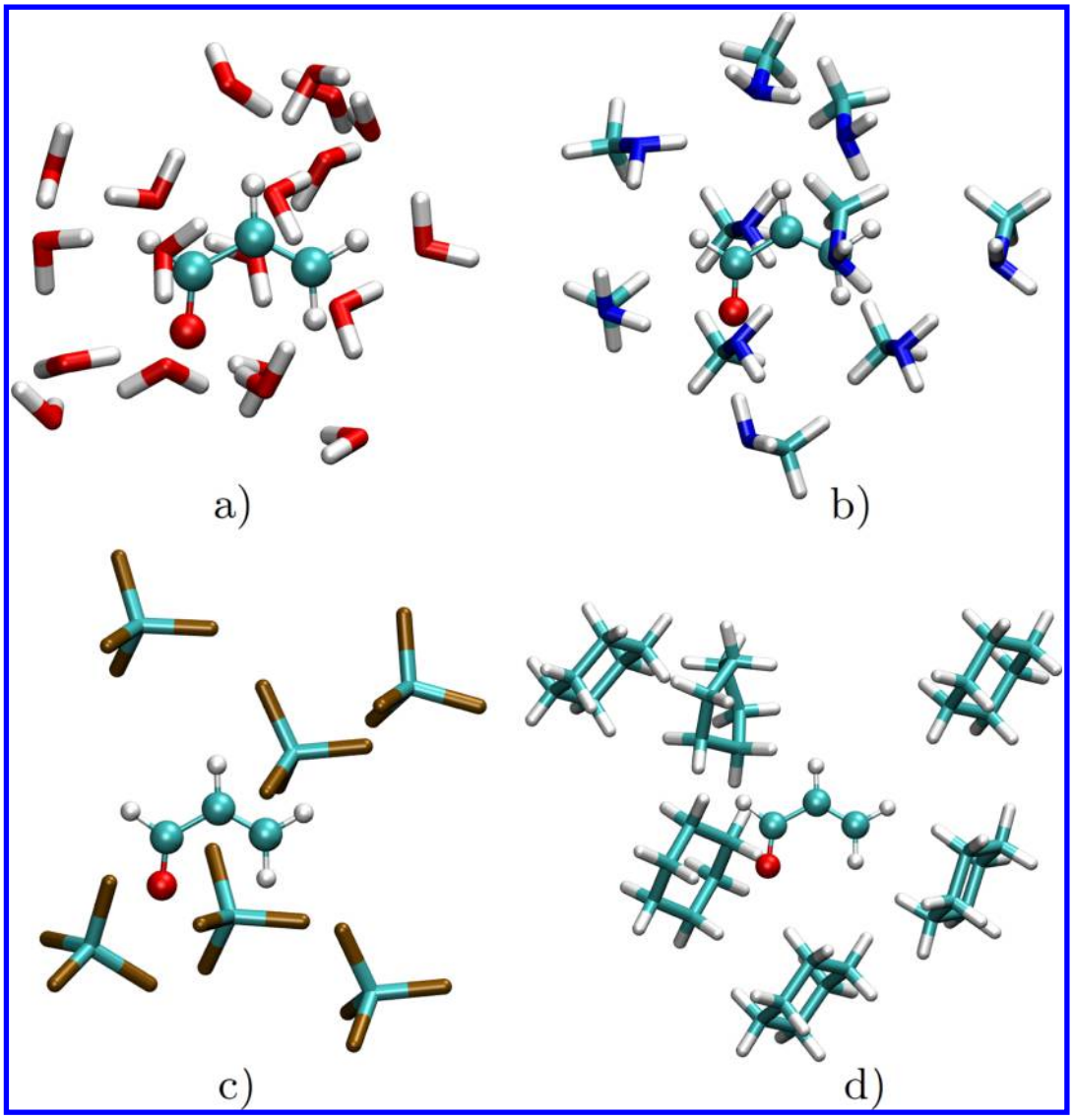

Figure 2. Cluster models with acrolein solvated in (a) water, (b) methylamine (CH_3NH_2), (c) carbon-tetrachloride (CCl_4), and (d) cyclohexane (C_6H_{12}).

Table 2. Excitation Energies (eV) of PNA and Acrolein in Different Solvents[a]

molecule		transition	solvent	QM/MM	$\Delta E^{(A)}$	$\delta E^{(A)}_{tot}$	scp-KS		fr-KS		ΔE_{super}
							$\Delta E^{(B)}$	$\delta E^{(B)}_{tot}$	$\Delta E^{(B)}$	$\delta E^{(B)}_{tot}$	
PNA	1	$\pi \rightarrow \pi^*$	H_2O	3.81	3.70	0.001	3.48	−0.84	3.55	−0.44	3.46
	2			3.67	3.54	0.001	3.48	−0.45	3.48	0.11	3.34
	3			3.61	3.46	0.001	3.47	−0.50	3.44	0.10	3.27
Acrolein		$n \rightarrow \pi^*$	H_2O	4.31	4.59	0.009	4.58	−5.29	no conv.		4.69
			CH_3NH_2		3.79	0.005	3.90	−2.55	no conv.		3.79
			CCl_4		3.66	0.003	3.66	0.03	no conv.		3.66
			C_6H_{12}		3.64	0.002	3.71	−1.69	3.65	−0.53	3.66
		$\pi \rightarrow \pi^*$	H_2O	5.65	5.76	0.007	5.76	2.53	5.76	0.96	5.70
			CH_3NH_2		5.98	0.004	5.94	0.85	5.96	0.17	5.95
			CCl_4		5.97	0.008	5.97	−0.36	5.97	−0.22	6.01
			C_6H_{12}		5.93	0.001	5.89	0.83	5.91	0.35	6.00

[a]The WF/DFT excitation energies, $\Delta E^{(A)}$ and $\Delta E^{(B)}$, are computed with a state-independent and a state-dependent embedding potential, respectively. The supermolecular excitation energies are denoted as ΔE_{super}. For scheme (B), we report the results obtained with two different excited-state DFT densities, scp-KS and fr-KS, to generate the excited-state embedding potential for the WF calculation. We also list the energy corrections, $\delta E^{(A)}_{tot}$ and $\delta E^{(B)}_{tot}$, which must be added to the simple WF eigenvalue differences to obtain the excitation energies given here. All excitation energies are computed with the CASPT2 approach.

dx.doi.org/10.1021/ct400086a | J. Chem. Theory Comput. 2013, 9, 2355−2367

the fr-KS case, we relax the orbitals at fixed fractional occupations until convergence.

We then keep the molecule in the chosen excited-state density and relax the environment in the ground state. Subsequently, we freeze the environment and find a new excited-state density of the solvated molecule by relaxing the orbitals either in the ground state or with fixed fractional occupations for the scp-KS and the fr-KS case, respectively. We repeat these steps (generating the excited-state density and relaxing the environment around the excited molecule) in cycles until the densities of the environment and of the solvated molecule are converged. We find that 5−6 cycles suffice for convergence for all systems.

4.2. Nitroaniline and Acrolein. We employ the WF/DFT embedding schemes with a state-independent (A) and a state-specific (B) embedding potential to compute the excitation energies $\Delta E^{(A)}$ and $\Delta E^{(B)}$ (eqs 19 and 21) of solvated PNA and acrolein. For scheme (B), we compute two sets of WF/DFT excitation energies corresponding to the two different embedding potentials we generate with the use of the scp-KS and the fr-KS excited-state DFT density for the active region. In all cases, we also evaluate the corrections which must be added to the simple excitation energies obtained as eigenvalue differences of the solute Hamiltonian including the embedding potential (eqs 15 and 22). We denote these energy contributions as

$$\begin{aligned} \delta E_{\mathrm{tot}}^{(A)} &= \delta E_{\mathrm{nadd}}^{(A)} \\ \delta E_{\mathrm{tot}}^{(B)} &= \delta E_{\mathrm{nadd}}^{(B)} + \delta E_{\mathrm{simple}}^{(B)} \end{aligned} \tag{28}$$

where we make use of eqs 20, 26, and 27. Then, in the case of water solvent, for which standard force fields are available, we consider a conventional QM/MM approach where the solvation shell is represented in terms of a nonpolarizable point-charge model as it is often done for complex biological or solvated systems. Finally, we perform a supermolecular calculation where the whole system is treated at the WF level, which provides a reference value for the other types of embedding. We collect all results in Table 2.

For PNA in water, we consider three structures of the model cluster corresponding to different steps during the geometry optimization, with the last structure (geometry 3) being the converged geometry of lower energy. For all structures, we find that already scheme (A) gives a better accuracy than the simple point-charge model, reducing the excitation energies by about 0.1−0.15 eV and bringing them into better agreement with the supermolecular values. The use of scheme (B) in the variant which includes the correction to the eigenvalue difference of the state-specific WF calculations further improves the excitation energies. On the other hand, the neglect of the corrections in scheme (B) would yield significantly worse results. In fact, while these terms are rather small in case (A) where they only include differential nonadditive contributions (eqs 20), they can instead be non-negligible in case (B). Furthermore, they also appear to depend rather strongly on the particular choice of excited-state DFT density for the generation of the excited-state embedding potential, being consistently smaller in the case of the so-called fr-KS density. Perhaps surprisingly, the excitation energies in scheme (B) including these corrections are instead rather independent of the particular choice of excited-state DFT density employed.

The best performance of scheme (B) is observed in correspondence with geometry 1. To understand how (B) improves upon (A), we can inspect the difference $v_{\mathrm{emb},1}^{\mathrm{pol,e}}(\mathbf{r}) - v_{\mathrm{emb},1}(\mathbf{r})$ between the excited-state embedding potential used in the WF excited-state calculation of case (B) and the ground-state potential used both in case (A) and in the WF ground-state calculation of case (B), which is shown in Figure 3. We

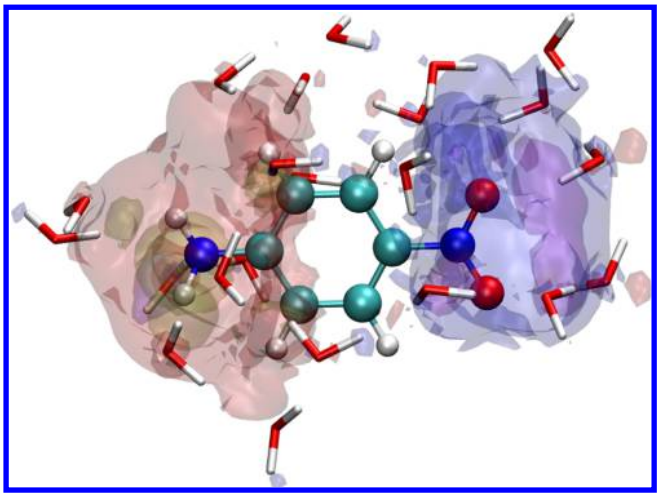

Figure 3. Difference of the state-specific excited- and ground-state embedding potentials for PNA (geometry 1). The excited-state potential is obtained with the use of the scp-KS excited-state density. The contours in violet, blue, red, and yellow correspond to the values of −0.02, −0.01, +0.01, and +0.02 au, respectively.

observe that the excited-state potential is more negative than the ground-state potential in the region close to the nitro group while the opposite holds in proximity of the amine group. Consequently, since the excitation implies a transfer of charge from the amine to the nitro group, the excited-state embedding potential will stabilize the excited state more than the ground-state, resulting in a lower excitation energy in scheme (B) than in (A).

An analysis of the results for structures 2 and 3 leads to qualitatively similar observations, but the improvement of the corrected case (B) compared to case (A) is diminished along the sequence of structures 1, 2, 3. In particular, for geometry 3, the (A) and (B) excitation energies are very similar, superior to the QM/MM value but about 0.2 eV higher than the supermolecular result. Since geometries 1, 2, and 3 represent a succession of structures along a geometry optimization with the last one being a minimum, it is possible that the nature of the hydrogen bonds changes as the structure reaches equilibrium, rendering the partitioning in different regions not adequate for the present case. To investigate this hypothesis, we compute the QM/MM, (A), and (B) excitation energies of structure 3, including some water molecules in the active region which are depicted in Figure 4. As reported in Table 3, when the waters close to the amino group are included in the active region and treated at the WF level, the agreement with the supermolecular calculation improves and the (A) and (B) excitation energies become well within 0.1 eV of the supermolecular value, with (B) being in better agreement that (A). Therefore, as conjectured, moving the partition between the two parts further away from the active systems and allowing a better description of relevant hydrogen bonds significantly improves the performance of the (A) and, in particular, the (B)

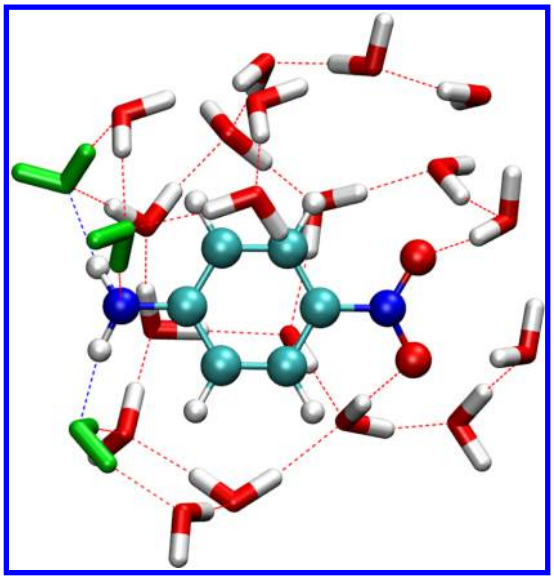

Figure 4. PNA and its solvation shell of 22 water molecules for structure 3. We depict in green the three water molecules added to the active region in Table 3.

Table 3. Excitation Energies (eV) of PNA in Water (geometry 3), Computed with Different Numbers of Water Molecules Included in the Active Region and Treated at the WF Level[a]

			ΔE_B	
active H_2O	QM/MM	ΔE_A	scp-KS	fr-KS
0	3.61	3.46	3.47	3.44
3	3.51	3.36	3.34	3.32
22 (all)	3.27	3.27	3.27	3.27

[a]The supermolecular computation is the limit of all four methods when all 22 water molecules are in the active system. For the notation, see the caption of Table 2.

scheme. Finally, while including these water molecules in the active part also improves the QM/MM excitation energy, the QM/MM value remains 0.24 eV higher than the supermolecular reference.

In Table 2, we also list the (A) and (B) excitation energies of acrolein in water and in the three other solvents shown in Figure 2. For case (B), we compute the excited-state potentials starting from the scp-KS and the fr-KS excited-state DFT densities. Perhaps not surprisingly, we find that the second procedure presents problems of convergence for the $n \rightarrow \pi^*$ excitation, where the construction of the density does not follow the Aufbau principle. We do instead not encounter such problems in the case of the $\pi \rightarrow \pi^*$ excitation, which corresponds to the HOMO−LUMO transition in KS-DFT.

For the $\pi \rightarrow \pi^*$ transition of acrolein in all solvents, the two sets of (B) excitation energies are always similar, and rather close to both the (A) and the supermolecular values. Therefore, differential polarization does not appear to play a significant role in the description of this transition even though some of the solvents would have been expected to strongly interact with the π electronic system of acrolein. This observation can be extended to the $n \rightarrow \pi^*$ transition where the (A) excitation energies are already in good agreement with the corresponding supermolecular calculation. In fact, for the $\pi \rightarrow \pi^*$ case, the use of scheme (B) with the scp-KS density slightly worsens the agreement with the reference values in the case of acrolein solvated in methylamine and cyclohexane. We note that, for cyclohexane, the use of a state-specific excited-state embedding potential constructed with the fully relaxed DFT excited-state density improves upon the scp-KS-based result, restoring the (A) value and the good agreement with the supermolecular calculation. We will further comment on the choice of excited-state DFT density for the construction of state-specific potentials below.

Finally, the energy corrections used in scheme (B) are always substantial for acrolein, being as large as 5 eV for $n \rightarrow \pi^*$ transition in water and the scp-KS case. Consequently, the excitation energies computed without these corrections as the eigenvalue difference of the state-specific Hamiltonians of the solute would be totally unreasonable. We note that the corrections to compute the (B) excitation energies based on the fr-KS density are systematically smaller that those based on

Table 4. Excitation Energies (eV) Computed with Scheme (B)[a]

solute		transition	solvent	$\Delta E^{(B)}_{approx}$	$\delta E^{(B)}_{simple}$	$\delta E^{(B)}_{nadd}$	$\Delta E^{(B)}$
PNA	1	$\pi \rightarrow \pi^*$	H_2O	4.32	−0.85	0.005	3.48
	2			3.93	−0.46	0.005	3.48
	3			3.98	−0.51	0.005	3.47
acrolein		$n \rightarrow \pi^*$	H_2O	9.88	−5.27	−0.023	4.58
			CH_3NH_2	6.46	−2.54	−0.013	3.90
			CCl_4	3.62	0.03	0.003	3.66
			C_6H_{12}	5.41	−1.68	−0.007	3.71
		$\pi \rightarrow \pi^*$	H_2O	3.23	2.54	−0.012	5.76
			CH_3NH_2	5.08	0.85	−0.002	5.94
			CCl_4	6.33	−0.36	0.001	5.97
			C_6H_{12}	5.07	0.83	−0.004	5.89
MCP		$\pi \rightarrow \pi^*$	H_2O	5.18	−0.48	−0.045	4.66
PNP	1	$\pi \rightarrow \pi^*$	H_2O	17.03	−12.75	0.003	4.28
	2			16.45	−12.29	0.006	4.17
	3			14.95	−10.85	0.010	4.11

[a]The energy corrections are split in the nonadditive and remaining contributions, which must be added to the eigenvalue differences of state-specific WF calculations ($\Delta E^{(B)}_{approx}$) to obtain the correct excitation energies ($\Delta E^{(B)}$). The scp-KS excited-state DFT density is used in the generation of the state-specific embedding potential.

Table 5. Excitation Energies and Energy Corrections (Nonadditive and Remaining Contributions, eV) of the MCP and PNP (Geometry 3) Molecules in Water Solvents, Obtained in a Supermolecular, QM/MM, (A), and (B) Calculations[a]

method	density	HOMO-1	HOMO	LUMO	LUMO+1	ΔE	δE_{simple}	δE_{nadd}
				MCP				
super						5.03		
QM/MM						4.88		
A		2	2	0	0	5.08		0.017
B	scp-KS	2	1	1	0	4.66	−0.48	−0.045
B	fr-KS (1)	2	1	1	0	4.81	0.12	−0.035
B	fr-KS (2)	1.9	1	1	0.1	4.87	−0.82	−0.036
				PNP				
super						3.50		
QM/MM						3.51		
A		2	2	0	0	3.49		0.001
B	scp-KS	2	1	1	0	4.11	−10.85	0.010
B	fr-KS (1)	2	1	1	0	3.72	−4.79	0.009
B	fr-KS (2)	1.9	1.2	0.8	0.1	3.67	−4.07	0.007

[a]In scheme (B), we employ the scp-KS and fr-KS excited-state densities obtained with (1) standard HOMO−LUMO and (2) fractional occupations over the HOMO−1, HOMO, LUMO, and LUMO+1 KS orbitals. The corresponding natural-orbital occupation numbers of the excited-state CASSCF wave function obtained in scheme (A) are (1.94, 1.01, 1.00, 0.06) and (1.88, 1.17, 0.87, 0.12) for MCP and PNP, respectively.

the scp-KS density. Finally, as for PNA, the use of eigenvalue differences of the solute Hamiltonian including the embedding potential is justified for scheme (A) since the energy corrections (computed as differences of nonadditive quantities) are always smaller than 0.01 eV.

4.3. Correction and Nonadditive Contributions. In Table 4, we analyze in more detail the energy corrections (eqs 26 and 27) which must be added to the eigenvalue differences of the state-specific WF calculations to obtain the final (B) excitation energy. In addition to PNA in water and acrolein in the four different solvents, we consider the MCP and PNP molecules in water and focus on the excitation energies obtained with the use of the scp-KS excited-state density since it is possible to converge this DFT density for all cases reported in the table.

We observe that, similarly to what was found for scheme (A), the nonadditive contributions are rather small, usually less than 0.02 eV, also in scheme (B). Therefore, the largest component in the energy corrections to the eigenvalue difference of state-specific solute Hamiltonians comes from the KS energy difference of the environment, being polarized in the ground and the excited state of the active part, plus the difference of the nuclear interaction of the active fragment with these two environmental densities. This contribution can be remarkably large and, in the case of PNP in three different water clusters, amounts to as much as −11 eV, greatly exceeding in absolute value the (B) excitation energy of about 4 eV. It is remarkable that the addition of such large energy corrections to a grossly incorrect eigenvalue difference leads to very reasonable excitation energies. As already mentioned and also shown below, it is even more remarkable that different procedures to compute the excited-state density in the generation of the state-specific potentials leads to very different eigenvalue differences and energy corrections, but remarkably close final excitation energies.

4.4. Construction of Excited-State DFT Density. We discuss here in more detail the choice of excited-state density for the active site employed to polarize the other fragments and construct a state-specific embedding potential for the WF excited-state calculation. To understand how this choice affects the (B) excitation energies, we consider the MCP and PNP molecules in water solvent, and in addition to the scp-KS and the fr-KS densities, we construct excited-state densities of the active region with fractional occupations over the HOMO−1, HOMO, LUMO, and LUMO+1 orbitals. The occupation numbers are based on the occupations of the natural orbitals of the excited-state wave function obtained in the CASSCF calculations, and the KS density is then relaxed in the spirit of the fr-KS density introduced before. The results are summarized in Table 5. We stress that the densities with fractional occupations are constructed to test the sensitivity of the result to the choice of approximate excited-state DFT density and are not proposed as a general practical route for scheme (B).

For both molecules, the (A) excitation energy is in very good agreement with the corresponding supermolecular calculation, and even an MM description of the environment appears to be sufficiently accurate. Therefore, differential polarization effects due to the response of the environment to the excitation of the active region are surely expected to be negligible. Nevertheless, scheme (B) with the use of the scp-KS density modifies the (A) excitation energy, significantly worsening the agreement of the WF/DFT approach with the reference. To understand whether this is a fundamental failure of scheme (B) or a problem with the construction of the approximate excited-state density needed in scheme (B), we compute the (B) excitation energies based on (1) the HOMO−LUMO fully relaxed density employed also above and (2) the fully relaxed density with fractional occupations. We find that the (B) excitation energy improves as we move from the scp-KS to the fr-KS (1) and the fr-KS (2) density, with the error with respect to the supermolecular value being reduced from 0.4 to 0.5 eV to less than 0.2 eV. Finally, as a consistency check, we consider two cases, PNA and the $\pi \rightarrow \pi^*$ transition of acrolein, where scp-KS and fr-KS densities yield similar (B) excitation energies and verify the robustness of this agreement by also constructing fully relaxed excited-state densities with fractional occupations inspired by the CASSCF wave functions. As shown in the Supporting Information, the use of fractional occupations in the excited-state DFT density does not affect the (B) excitation energy of these two systems, supporting the idea that the equivalent performance of the scp-KS and fully relaxed

HOMO−LUMO density is a good indicator of the robustness of the (B) results for the particular system under study.

To investigate more closely the relative accuracy of the scp-KS and fr-KS procedures employed to obtain the excited-state density of the active molecule, we compare the difference between the ground- and excited-state densities computed within subsystem DFT and CASPT2 for MCP in water. As seen above, this molecule represents a good test case since the use of these two excited-state densities leads to different (B) excitation energies, with the values obtained with the fr-KS density being in better agreement with the supermolecular reference. As DFT densities for the total system, we use the sum of the densities of the molecule and the environment obtained self-consistently for each subsystem (a comparison of the densities of only the active subsystem is included in the Supporting Information). The CASPT2 densities are computed with the first-order wave function from a supermolecular calculation (and therefore also include some second-order contributions) and are here obtained through perturbative calculations on top of state-specific CASSCF wave functions separately targeting the ground and the excited state. For the vertical excitation of MCP in water, the use of state-specific CASSCF energies is robust as the energy difference between the ground and excited states is large and, furthermore, the corresponding wave functions of the nearly planar molecule preserve approximately different symmetry character. On the other hand, the use of state-average orbitals leads to CASSCF densities of significantly lower quality and therefore to less reliable CASPT2 densities, as discussed in more detail in the Supporting Information.

In Figure 5, we plot the difference between the excited- and ground-state densities integrated over cross sections normal to

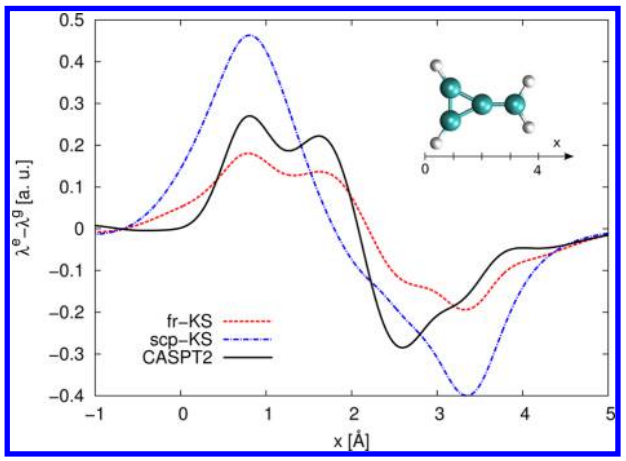

Figure 5. Difference between the excited- and ground-state densities of MCP in water, integrated over planes perpendicular to the x axis (eq 29) and computed with CASPT2 and the approximate subsystem DFT schemes.

the axis formed by the two carbon atoms of the CCH_2 terminus (defined here as the x axis):

$$\lambda^{e}(x) - \lambda^{g}(x) = \int \rho^{e}(x, y, z)\, dy\, dz - \int \rho^{g}(x, y, z)\, dy\, dz \tag{29}$$

We observe that both approximate DFT densities correctly display the general feature that charge transfer occurs from the ethylene moiety to the ring but differ significantly in describing the extent of the change. In particular, the scp-KS procedure leads to a more marked transfer of charge which mainly interests the extremes of the molecule, while the fr-KS density is more structured and better reproduces the general features of the CASPT2 reference. Therefore, the improvement observed in the fr-KS excitation energy of MCP as compared to the scp-KS value coincides with a superior description of the excited-state density employed to construct the state-specific excited-state embedding potential for the WF calculation. Similarly, we have found that also for PNP, the fr-KS density is of better quality than the scp-KS one. It is however clear that alternative strategies must be devised for the construction of the excited-state density since non-negligible differences remain between the fr-KS and the reference density, and between the corresponding (B) excitation energy and the supermolecular value. Furthermore, we must recall that the fr-KS scheme may suffer from convergence problems for non-Aufbau excited-state densities as shown above for the $n \rightarrow \pi^*$ excitation of acrolein.

Finally, we observe that the use of different excited-state DFT densities in scheme (B) can lead to quite large and different energy corrections (eq 25) as shown in Table 5. For instance, in the case of PNP, the corrections corresponding to the scp-KS and fr-KS densities are −10.85 and −4.79 eV, respectively, and, therefore, differ by as much as 6 eV. This remarkable difference is however diminished when the corrections are added to the eigenvalue differences of the state-specific Hamiltonians (eq 22). The final excitation energies of PNP in scheme (B) are in fact rather similar for the two choices of excited-state densities, and equal to 4.11 and 3.72 eV, respectively.

To understand the reasons behind this cancellation, we rewrite the expression of the eigenvalue difference (eq 22) neglecting the small nonadditive contributions as

$$\begin{aligned}\Delta E^{(B)}_{\text{approx}} &\approx E_1^{\text{WF}}[\Psi_1^{\text{pol,e}}] - E_1^{\text{WF}}[\Psi_1^{\text{g}}] + V_{\text{nuc,2}}[\rho_1^{\text{pol,e}}] \\ &\quad - V_{\text{nuc,2}}[\rho_1^{\text{g}}] + J[\rho_1^{\text{pol,e}}, \rho_2^{\text{pol}}] - J[\rho_1^{\text{g}}, \rho_2] \\ &= E_1^{\text{WF}}[\Psi_1^{\text{pol,e}}] - E_1^{\text{WF}}[\Psi_1^{\text{g}}] + \int v_{\text{nuc,2}}(\mathbf{r})\Delta\rho_1(\mathbf{r})\, d\mathbf{r} \\ &\quad + J[\rho_1^{\text{g}}, \Delta\rho_2] + J[\rho_2, \Delta\rho_1] + J[\Delta\rho_1, \Delta\rho_2]\end{aligned} \tag{30}$$

where $\Delta\rho_1(\mathbf{r}) = \rho_1^{\text{pol,e}}(\mathbf{r}) - \rho_1^{\text{g}}(\mathbf{r})$. The last term is relatively small compared to the other electrostatic terms, and the first WF energy difference is expected to be not so sensitive to changes in the embedding potential, which only affect the expectation value through changes in the excited-state wave function of system 1. Furthermore, the second term describing the interaction of nuclei of system 2 with $\Delta\rho_1$ will largely cancel the electrostatic interaction $J[\rho_2,\Delta\rho_1]$. Therefore, the only term in the expression above which may significantly vary with changes in $\Delta\rho_2$ is $J[\rho_1^{\text{g}}, \Delta\rho_2]$.

We then observe that the leading term in the energy correction (eq 25) is the interaction of the nuclei of active system 1 with the density difference $\Delta\rho_2$ of the environment. We expect this contribution to largely cancel the electrostatic interaction of ρ_1^{g} with $\Delta\rho_2$ in the equation above, namely,

$$\int v_{\text{nuc,1}}(\mathbf{r})\, \Delta\rho_2(\mathbf{r})\, d\mathbf{r} + J[\rho_1^{\text{g}}, \Delta\rho_2] \approx 0 \tag{31}$$

to zeroth order. Therefore, the final excitation energy obtained by adding the energy correction (eq 25) to the eigenvalue difference (eq 22) will vary less than the correction and the eigenvalue difference itself, when different excited-state DFT densities are employed to polarize the environment and construct the state-specific embedding potential. To illustrate

this cancellation in PNP, we note that the interaction of the nuclei of system 1 with $\Delta\rho_2$ is equal to −10.74 and −4.69 eV in correspondence with the scp-KS and the fr-KS excited-state density and amounts to almost the full energy correction of −10.85 and −4.79 eV, respectively. Furthermore, these contributions largely cancel the corresponding terms, $J[\rho_1^g, \Delta\rho_2]$, which are of opposite sign and equal to 11.10 and 4.85 eV.

5. CONCLUSIONS

In this work, we have outlined a practical route to compute the excitation energies of a molecule embedded in a responsive environment within a WF/DFT scheme that can account for the mutual polarization of the fragments upon excitation of the active molecule. The approach relies on the construction of state-specific embedding potentials within an approximate subsystem DFT approach we have adapted to treat the active fragment in its excited state. We have evaluated the explicit energy expression of the total system in the ground and excited states, using both state-independent and state-dependent embedding potentials, that is, either freezing or relaxing the environment in response to the excitation of the embedded molecule.

We showed that, if state-independent embedding potentials are used (frozen environment), computing the excitation energies as WF eigenvalue differences of the Hamiltonian of the active molecule with included the embedding potential yields an approximate, reasonable treatment of embedding effects. The reasons for the effectiveness of these energy expressions lie in the fact that the neglected terms are differences of nonadditive energy contributions, which are expected to be small. In contrast, if differential polarization effects are included in terms of state-dependent embedding potentials (responsive environment), we demonstrated that a simple correction must be added to the WF eigenvalue differences of the state-specific Hamiltonians of the embedded molecule, since important Coulomb contributions would otherwise be neglected. The uncorrected calculations with state-specific embedding potentials result in fact in significantly worse excitation energies than with state-independent embedding potentials while the corrected expression may bring the state-specific results into better agreement with the supermolecular reference values. Also in the case of state-dependent embedding potentials, the neglect of nonadditive contributions in the evaluation of the excitation energies does not appreciably affect the results.

We demonstrated all these concepts with the state-independent and state-dependent computation of the excitation energies of *p*-nitroaniline, acrolein, methylenecyclopropene, and *p*-nitrophenolate in various solvents. We showed that the use of state-independent potentials generally improves on a QM/MM description. It is also often sufficient to obtain excitation energies in good agreement with the supermolecular values, surprisingly also in the case of *p*-nitrophenolate in water where calculations with polarizable force fields have instead reported large contributions to the energies from the polarization of the solvent upon excitation of the molecule. For *p*-nitroaniline, we found instead that mutual polarization effects are important and that the use of state-specific embedding can improve the description of the excitation energies of this system.

Finally, when using state-dependent potentials, we found that a key ingredient is the choice of excited-state density for the active part, which we employ to polarize the other fragments and construct a state-specific embedding potential for the WF excited-state calculation. We have outlined ways to obtain approximate excited-state densities in terms of embedded KS-DFT calculations (also with non-Aufbau occupation numbers), but when these approximate densities result in rather different excitation energies as in the case of methylenecyclopropene and *p*-nitrophenolate, we take this as indicating that a better description of the excited-state density is needed, possibly through a WF calculation. This particular issue will require further investigation and will be the subject of future studies.

■ ASSOCIATED CONTENT

Supporting Information

Excitation energies of the isolated molecules. Results obtained with fractional occupations for the excited-state densities of PNA and acrolein. Comparison and discussion of state-average and state-specific CASSCF and CASPT2 densities. Comparison of the DFT and CASPT2 densities of only the active subsystem. This material is available free of charge via the Internet at http://pubs.acs.org.

■ AUTHOR INFORMATION

Corresponding Author

*E-mail: j.neugebauer@uni-muenster.de; c.filippi@utwente.nl.

Notes

The authors declare no competing financial interest.

■ ACKNOWLEDGMENTS

C.D. is supported by an ECHO grant (712.011.005) and J.N. by a VIDI grant (700.59.422) of The Netherlands Organisation for Scientific Research (NWO). We acknowledge a computer time grant from the Stichting Nationale Computer Faciliteiten (NCF). We thank C. Angeli for useful discussions. We would also like to thank E. Carter for making an initial version of the WF/DFT interface for the Molcas program available to us. Support by COST Action CODECS is acknowledged.

■ REFERENCES

(1) Senn, H. M.; Thiel, W. *Angew. Chem., Int. Ed.* **2009**, *48*, 1198−1229.
(2) Svensson, M.; Humbel, S.; Froese, R. D. J.; Matsubara, T.; Sieber, S.; Morokuma, K. *J. Phys. Chem.* **1996**, *100*, 19357−19363.
(3) Fedorov, D. G.; Kitaura, K. *J. Phys. Chem. A* **2007**, *111*, 6904−6914.
(4) Gordon, M. S.; Fedorov, D. G.; Pruitt, S. R.; Slipchenko, L. V. *Chem. Rev.* **2012**, *112*, 632−672.
(5) Neugebauer, J. *Phys. Rep.* **2010**, *489*, 1−87.
(6) Dreuw, A.; Head-Gordon, M. *Chem. Rev.* **2005**, *105*, 4009−4037.
(7) Gomes, A. S. P.; Jacob, C. R. *Annu. Rep. Prog. Chem., Sect. C* **2012**, *108*, 222−277.
(8) Jensen, L.; van Duijnen, P. T.; Snijders, J. G. *J. Chem. Phys.* **2003**, *119*, 3800−3809.
(9) Sneskov, K.; Schwabe, T.; Christiansen, O.; Kongsted, J. *Phys. Chem. Chem. Phys.* **2011**, *13*, 18551−18560.
(10) Lipparini, F.; Cappelli, C.; Barone, V. *J. Chem. Theory Comput.* **2012**, *8*, 4153−4165.
(11) Senatore, G.; Subbaswamy, K. R. *Phys. Rev. B* **1986**, *34*, 5754−5757.
(12) Cortona, P. *Phys. Rev. B* **1991**, *44*, 8454−8458.
(13) Iannuzzi, M.; Kirchner, B.; Hutter, J. *Chem. Phys. Lett.* **2006**, *421*, 16−20.
(14) Wesolowski, T. A.; Warshel, A. *J. Phys. Chem.* **1993**, *97*, 8050−8053.

(15) Wesolowski, T. A.; Weber, J. *Chem. Phys. Lett.* **1996**, *248*, 71−76.
(16) Wesolowski, T. A. One-electron Equations for Embedded Electron Density: Challenge for Theory and Practical Payoffs in Multi-Level Modeling of Complex Polyatomic Systems. In *Computational Chemistry: Reviews of Current Trends*; Leszczynski, J., Ed.; World Scientific: Singapore, 2006; Vol. *10*, pp 1−82.
(17) Casida, M. E.; Wesolowski, T. A. *Int. J. Quantum Chem.* **2004**, *96*, 577−588.
(18) Neugebauer, J. *J. Chem. Phys.* **2007**, *126*, 134116.
(19) Neugebauer, J.; Curutchet, C.; Muños-Losa, A.; Mennucci, B. *J. Chem. Theory Comput.* **2010**, *6*, 1843−1851.
(20) Govind, N.; Wang, Y. A.; da Silva, A. J. R.; Carter, E. A. *Chem. Phys. Lett.* **1998**, *295*, 129−134.
(21) Govind, N.; Wang, Y. A.; Carter, E. A. *J. Chem. Phys.* **1999**, *110*, 7677−7688.
(22) Wesolowski, T. A. *Phys. Rev. A* **2008**, *77*, 012504.
(23) Huang, P.; Carter, E. A. *J. Chem. Phys.* **2006**, *125*, 084102.
(24) Roncero, O.; de Lara-Castells, M. P.; Villarreal, P.; Flores, F.; Ortega, J.; Paniagua, M.; Aguado, A. *J. Chem. Phys.* **2008**, *129*, 184104.
(25) Roncero, O.; Zanchet, A.; Villarreal, P.; Aguado, A. *J. Chem. Phys.* **2009**, *131*, 234110.
(26) Huang, C.; Carter, E. A. *J. Chem. Phys.* **2011**, *135*, 194104.
(27) Aquilante, F.; Wesolowski, T. A. *J. Chem. Phys.* **2011**, *135*, 084120.
(28) Manby, F. R.; Stella, M.; Goodpaster, J. D.; Thomas F. Miller, I. *J. Chem. Theory Comput.* **2012**, *8*, 2564−2568.
(29) Since different partitionings of the electron density can be adopted within subsystem density functional theory,[16,65] we use the term "polarization" with respect to the situation of no interaction, namely, the isolated case. We note that the notion of polarization is not ambiguous if a unique embedding potential can be achieved for all subsystems as shown by Elliott et al.[66,67] within DFT-in-DFT and transferred to WF-in-DFT methods by Huang et al.[26,68]
(30) Klüner, T.; Govind, N.; Wang, Y. A.; Carter, E. A. *Phys. Rev. Lett.* **2001**, *86*, 5954−5957.
(31) Klüner, T.; Govind, N.; Wang, Y. A.; Carter, E. A. *J. Chem. Phys.* **2002**, *116*, 42−54.
(32) Khait, Y. G.; Hoffmann, M. R. *J. Chem. Phys.* **2010**, *133*, 044107.
(33) Sharifzadeh, S.; Huang, P.; Carter, E. A. *J. Phys.: Condens. Matter* **2009**, *21*, 355501.
(34) Kanan, D. K.; Sharifzadeh, S.; Carter, E. A. *Chem. Phys. Lett.* **2012**, *519*−*520*, 18−24.
(35) Höfener, S.; Gomes, A. S. P.; Visscher, L. *J. Chem. Phys.* **2012**, *136*, 044104.
(36) We note that the use of an approximate WF method (as opposed to the full configuration interaction limit) does not lead to the ground-state energy of the total system but to an upper bound. Also in the case of a frozen environmental density (system 2) which is larger than the exact total density in some region of space, the minimization with respect to the density of system 1 will only lead to an upper bound.[14,22] For the calculation of energy differences, this may lead to error cancellation, although this is not guaranteed.
(37) Gomes, A. S. P.; Jacob, C. R.; Visscher, L. *Phys. Chem. Chem. Phys.* **2008**, *10*, 5353−5362.
(38) Perdew, J. P.; Levy, M. *Phys. Rev. B* **1985**, *31*, 6264−6272.
(39) One can regard this approximation as related to the linearization of the embedding potential, which was shown in ref 69 to have only mild effects on orbital energies and other molecular properties in general. An advantage of using the same embedding potential for both electronic states is that the resulting wave functions are orthogonal and transition moments can be evaluated in a straightforward way. Note that this is not the case if the nonlinear terms are evaluated exactly, although deviations from orthogonality may be small in practice.
(40) Frisch, M. J.; Trucks, G. W.; Schlegel, H. B.; Scuseria, G. E.; Robb, M. A.; Cheeseman, J. R.; Scalmani, G.; Barone, V.; Mennucci, B.; Petersson, G. A.; Nakatsuji, H.; Caricato, M.; Li, X.; Hratchian, H. P.; Izmaylov, A. F.; Bloino, J.; Zheng, G.; Sonnenberg, J. L.; Hada, M.; Ehara, M.; Toyota, K.; Fukuda, R.; Hasegawa, J.; Ishida, M.; Nakajima, T.; Honda, Y.; Kitao, O.; Nakai, H.; Vreven, T.; Montgomery, J. A., Jr.; Peralta, J. E.; Ogliaro, F.; Bearpark, M.; Heyd, J. J.; Brothers, E.; Kudin, K. N.; Staroverov, V. N.; Kobayashi, R.; Normand, J.; Raghavachari, K.; Rendell, A.; Burant, J. C.; Iyengar, S. S.; Tomasi, J.; Cossi, M.; Rega, N.; Millam, J. M.; Klene, M.; Knox, J. E.; Cross, J. B.; Bakken, V.; Adamo, C.; Jaramillo, J.; Gomperts, R.; Stratmann, R. E.; Yazyev, O.; Austin, A. J.; Cammi, R.; Pomelli, C.; Ochterski, J. W.; Martin, R. L.; Morokuma, K.; Zakrzewski, V. G.; Voth, G. A.; Salvador, P.; Dannenberg, J. J.; Dapprich, S.; Daniels, A. D.; Farkas, Ö.; Foresman, J. B.; Ortiz, J. V.; Cioslowski, J.; Fox, D. J. *Gaussian 09*, Revision A.02; Gaussian Inc.: Wallingford, CT, 2009.
(41) Ahlrichs, R.; Bär, M.; Häser, M.; Horn, H.; Kölmel, C. *Chem. Phys. Lett.* **1989**, *162*, 165−169.
(42) Dunning, T. H., Jr. *J. Chem. Phys.* **1989**, *90*, 1007−1023.
(43) Becke, A. D. *J. Chem. Phys.* **1993**, *98*, 5648−5652.
(44) Stephens, P. J.; Devlin, F. J.; Chabalowski, C. F.; Frisch, M. J. *J. Phys. Chem.* **1994**, *98*, 11623−11627.
(45) Becke, A. D. *Phys. Rev. A* **1988**, *38*, 3098−3100.
(46) Lee, C.; Yang, W.; Parr, R. G. *Phys. Rev. B* **1988**, *37*, 785−789.
(47) *Amsterdam Density Functional Program*; Theoretical Chemistry, Vrije Universiteit: Amsterdam. URL: http://www.scm.com (access date: July 15, 2012).
(48) Zhao, Y.; Truhlar, D. G. *J. Phys. Chem. A* **2006**, *110*, 13126−13130.
(49) van Lenthe, E.; Baerends, E. J. *J. Comput. Chem.* **2003**, *24*, 1142−1156.
(50) Lembarki, A.; Chermette, H. *Phys. Rev. A* **1994**, *50*, 5328−5331.
(51) Wesolowski, T. A. *J. Chem. Phys.* **1997**, *106*, 8516−8526.
(52) Vosko, S. H.; Wilk, L.; Nusair, M. *Can. J. Phys.* **1980**, *58*, 1200−1211.
(53) Aquilante, F.; De Vico, L.; Ferré, N.; Ghigo, G.; Malmqvist, P.-Å.; Neogrády, P.; Pedersen, T. B.; Pitoňák, M.; Reiher, M.; Roos, B. O.; Serrano-Andrés, L.; Urban, M.; Veryazov, V.; Lindh, R. *J. Comput. Chem.* **2010**, *31*, 224−247.
(54) Sharifzadeh, S.; Huang, P.; Carter, E. A. *Chem. Phys. Lett.* **2009**, *470*, 347−352.
(55) Ghigo, G.; Roos, B. O.; Malmqvist, P.-Å. *Chem. Phys. Lett.* **2004**, *396*, 142−149.
(56) Forsberg, N.; Malmqvist, P.-Å. *Chem. Phys. Lett.* **1997**, *274*, 196−204.
(57) Aquilante, F.; Malmqvist, P.-Å.; Pedersen, T. B.; Ghosh, A.; Roos, B. O. *J. Chem. Theory Comput.* **2008**, *4*, 694−702.
(58) Kendall, R. A.; Dunning, T. H., Jr.; Harrison, R. J. *J. Chem. Phys.* **1992**, *96*, 6796−6806.
(59) Hehre, W. J.; Ditchfield, R.; Pople, J. A. *J. Chem. Phys.* **1975**, *56*, 2257−2261.
(60) Jorgensen, W. L.; Chandrasekhar, J.; Madura, J. D. *J. Chem. Phys.* **1983**, *79*, 926−935.
(61) Millefiori, S.; Favini, G.; Millefiori, A.; Grasso, D. *Spectrochim. Acta A* **1977**, *33*, 21−27.
(62) Kovalenko, S.; Schanz, R.; Farztdinov, V.; Hennig, H.; Ernsting, N. *Chem. Phys. Lett.* **2000**, *323*, 312−322.
(63) Moskvin, A. F.; Yablonskii, O. P.; Bondar, L. F. *Theor. Exp. Chem.* **1966**, *2*, 469−472.
(64) Staley, S. W.; Norden, T. D. *J. Am. Chem. Soc.* **1984**, *106*, 3700−3701.
(65) Savin, A.; Wesolowski, T. Orbital-Free Embedding Effective Potential in Analytically Solvable Cases. In *Advances in the Theory of Atomic and Molecular Systems*; Piecuch, P., Maruani, J., Delgado-Barrio, G., Wilson, S., Eds.; Springer: The Netherlands, 2009; Vol. *19*, pp 311−326.
(66) Elliott, P.; Cohen, M. H.; Wasserman, A.; Burke, K. *J. Chem. Theory Comput.* **2009**, *5*, 827−833.
(67) Elliott, P.; Burke, K.; Cohen, M. H.; Wasserman, A. *Phys. Rev. A* **2010**, *82*, 024501.
(68) Huang, C.; Pavone, M.; Carter, E. A. *J. Chem. Phys.* **2011**, *134*, 154110.
(69) Dulak, M.; Wesolowski, T. A. *J. Chem. Theory Comput.* **2006**, *2*, 1538−1543.